IEEE Access
Multidisciplinary | Rapid Review | Open Access Journal

Received May 17, 2021, accepted June 15, 2021, date of publication June 18, 2021, date of current version June 29, 2021.

Digital Object Identifier 10.1109/ACCESS.2021.3090360

Extended Geometric Feature Extraction Process for Detecting Multiple Frequency Oscillations in KEPCO System

HWANHEE CHO[1,2], (Member, IEEE), NAMKI CHOI[1], (Graduate Student Member, IEEE), SUCHUL NAM[3], (Member, IEEE), AND BYONGJUN LEE[1], (Senior Member, IEEE)

[1]School of Electrical and Electronics Engineering, Korea University, Seoul 02841, South Korea
[2]Smart Electrical Signaling Division, Electrification System Research Department, Korea Railroad Research Institute (KRRI), Uiwang 16105, South Korea
[3]Power Transmission Laboratory, Korea Electric Power Research Institute (KEPRI), Daejeon 34056, South Korea

Corresponding author: Byongjun Lee (leeb@korea.ac.kr)

This work was supported in part by the National Research Foundation of Korea (NRF) grant through the Korea Government [Minister of Science and ICT (MSIT)] under Grant NRF-2021R1A2C2006511, in part by the Human Resources Program in Energy Technology of the Korea Institute of Energy Technology Evaluation and Planning (KETEP), and in part by the Ministry of Trade, Industry and Energy (MOTIE) of the Republic of Korea under Grant 20204010600220.

ABSTRACT In this study, a new algorithm dealing with time-varying modes for determining and tracing multiple frequency oscillations in power systems is proposed. Multiple modes or resonance of forced and natural oscillations can have severe effects on a power system. Therefore, it is crucial to recognize the dominant natural and forced oscillations because the oscillation mode possesses time-varying features that depend on the system operating conditions or changes in the parameters. The salient features of the proposed algorithm include the use of a time-series-based approach to recognize undesired modes (including multiple oscillations over a wide frequency range), tracing time-varying modes as the power system operating condition changes, and effectively determining and applying the oscillation features before implementing the corresponding control measures in the power system. In this study, multiple frequency oscillation scenarios for the test system and practical measurement data for a recent incident that occurred in Korea Electric Power Corporation (KEPCO) system are discussed. Therefore, the proposed algorithm can be practically applied in wide-area monitoring systems, not only for a single forced oscillation or local mode detection but also for system-wide inter-area mode recognition.

INDEX TERMS Forced oscillation, mode tracing, multiple frequency oscillation, natural oscillation, time-varying modes.

I. INTRODUCTION

Power system oscillations are mainly produced by weak damping or periodic external input. The weak damped modes in the system can create natural oscillation, whereas the periodicity of the external inputs can cause forced oscillation. Resonances between forced and natural oscillations can result in undesired instability or operational problems [1], [2]; more specifically, they can have an adverse effect on the generators owing to the resonance between the forced oscillations and local modes, although natural and forced responses can be distinguished from each other [3], [4].

The associate editor coordinating the review of this manuscript and approving it for publication was Zhouyang Ren.

In contrast, with an increasing number of installed phasor measurement units (PMUs), it is feasible to detect these incidents using measurement-based approaches [5]. Numerous researchers have attempted to perform a post-event analysis in the frequency domain [6] or have used Prony-based methods [7], [8] for time-domain estimations. Meanwhile, the empirical technique of mode decomposition is widely studied for oscillation analysis associated with Hilbert-Huang Transformation (HHT) [9], [10]. Coherence-based techniques for distinguishing forced oscillations from natural oscillations are reported in [11]–[13]. In the operation center of the Bonneville Power Administration (BPA), a simple root-mean-square (RMS)-based energy filter was implemented to detect oscillations in multiple frequency bands [14]. The BPA

method is intuitive for the four types of natural oscillations; however, forced oscillations, which can be observed in every frequency band, are difficult to identify using this method. However, if the conditions of the measurement devices are sufficient for observing the oscillatory behavior addressed in [15], time-series techniques, such as the maximum Lyapunov exponent for near real-time oscillation detection, are available [16]. The aforementioned studies used signal-based estimators with a low oscillation feature capturing capability, which are specialized for ringdown or transient data types by directly adopting certain techniques to detect the components of interest in a measurement. This indicates that these estimation techniques are mainly used for transient, or ringdown power oscillations.

Estimation methods with a high oscillation feature capturing capability, which can handle both ambient and ringdown data types, have also been studied; these methods consist of adaptive and model-based features. There are some model-based methods based on dynamics which adopts reduced-order of grey-box model and estimate from measurements And these approaches called system identification [17]. But many of the methods adopt stochastic models to estimate oscillatory features. In [18], Kalman filtering (KF) techniques were introduced as a successful method for damping and frequency analysis in Europe. The use of KF techniques for oscillation detection was initially introduced in [19] and [20]. Eigenvalues of a converted continuous system were used in these studies, which has a changing tuning parameter for the n-th discrete model. In [21], the authors shared their experience with Nordic power systems using a KF technique for WAMS applications. Moreover, the authors of [22] introduced wavelet transformation with the random decrement (WTRD) technique [23], which can manage damping in the WT framework. These current adaptive monitoring techniques are well-defined time-varying analysis methods that can effectively characterize the oscillation features. However, KF can also yield false results (undesirable final error levels) if the model is imperfect [24]. More specifically, when using high-resolution data, such as data from PMUs (short time step), or unmodeled repeating external disturbances including forced oscillations, are involved. However, the authors in [25] presented a comparative study regarding power system mode estimation despite the presence of forced oscillation by using varying estimation models that are capable of handling exogenous input. In contrast, [26] introduced a process to recognize oscillatory behavior using geometrical feature extraction (GFE), which is a signal-based estimator with a high oscillation feature capturing capability. However, the aforementioned studies do not provide simple solutions to issues arising from multiple frequencies or resonances between forced and natural oscillations.

Furthermore, the detection of forced oscillation in power systems, which is characterized by low-frequency oscillation, has become a major problem. Several other methods have been proposed to extract spectral information using periodogram-based techniques [27]–[29]. In [30] and [31], the authors used self- or cross-coherence methods to detect when the oscillation begins. These methods use a spectral technique, allowing them to effectively distinguish between ambient signals and sustained oscillations. Furthermore, their high strength against multifrequency oscillation is also noteworthy. An envelope shape analysis was introduced in [32], considering that the envelope-shaped forced oscillations are distinguishable from those of natural oscillations. In [2], a covariance-based approach was used to detect and estimate both forced and natural oscillations. However, considering oscillation features have time-varying properties [33], a new oscillation recognition methodology is required to handle multifrequency or resonance issues. This study focuses on a multifrequency oscillation recognition process based on [26]. The extended application of the GFE process is enabled by using certain properties of a two-torus dynamical system in [34]. In this case, the radius of trajectory (RoT), obtained using the GFE process, is no longer constant; instead, its value periodically fluctuates. Therefore, this study uses multiple GFE steps to break down the original signal into several estimated modes.

The proposed expanded GFE (EGFE) process is motivated by analytical methods for the nonlinear dynamics of distinct phenomena, such as oscillations [35], [36]. These approaches are currently being revisited, considering the fact that certain phenomena can affect a weak grid or poorly damped system owing to inverter-based resources or cables [37]. The major advantages of the time-series-based algorithms for oscillation detection, such as the GFE process [26], are as follows:

1) Extraction of undesired multiple-mode frequencies and damping is possible using a time-series-based approach. This applies to post-mortem analysis and to the online PMU application.
2) The proposed method can track time-varying multifrequency modes, including continuous monitoring. Thus, by designing the EGFE structure based on [26], operators can monitor oscillations for not only ringdown or transient events, but also ambient oscillations (in regular operations).
3) Oscillatory behavior evaluation is possible for the observable inter-area modes, despite the presence of forced oscillations or local modes. More, specifically, EGFE effectively provides frequency and damping information, which can be used to determine when the control measures in the power systems should operate.

Note, certain poorly damped natural oscillations are related to problems at a particular plant, which are significantly similar to forced oscillations [38]. The determination of whether the oscillation is natural or forced is beyond the scope of this study. Thus, this study assumes that there is no need to distinguish between natural and forced oscillations, and these cases are considered to have an undesired mode with multiple frequency ranges. This assumption is possible because the proposed method mainly focuses on poorly damped oscillations as an object of practical interest for monitoring,

regardless of the forced/natural classification. The proposed method locally and partially considers the oscillation act as a response signal of the linear system. Thus, the terms *mode* and *multifrequency* in this study are only valid when defining and applying the EGFE process. Furthermore, this study discusses a recent oscillation event triggered by forced input in Korea Electric Power Corporation (KEPCO) systems owing to the commissioning of two units of a thyristor-controlled series capacitor (TCSC).

The Poincaré map for a two-torus problem associated with spline interpolation is introduced in Section II, which is followed by the discussion of the extended GFE structure using mathematical concepts. The oscillation recognition method with the proposed EGFE is applied to the composed multifrequency signal, followed by an evaluation of its accuracy. Then, the GFE is applied to the simulation results and practical power system measurements in Sections III and IV, respectively, which is followed by the Conclusion.

II. EXPANDED GEOMETRICAL FEATURE EXTRACTION PROCESS FOR MULTIPLE FREQUENCY OSCILLATION

The oscillation detection method was developed in [16] by adopting the MLE algorithm to consider the nonlinearity of the phenomena. The method considers useful mathematical conditions, such as the average system and Poincaré map [39], to enhance the universality of the oscillation recognition process [26]. In [26], salient features of the difference with respect to [16] in a mathematical context were provided. Furthermore, certain useful algorithms for a measurement-based nonlinear system analysis were defined and implemented to recognize oscillatory behavior based on power system measurements.

1) State Space Construction (SSC):

This algorithm consists of two parts.

- This step is important to represent time series data as a two-dimensional system via periodic delay. The initial delay setting is updated upon each return of the trajectory.

$$f_c(t, x(t), \varepsilon) \rightarrow f_d(k, X(k), X(k-\delta)), \tag{1}$$

  where the function f_c is the desired system for which the oscillation response, depicted by changing the constant ε, needs to be estimated; f_d is a generated function with measured $X(k)$ and buffered $Y(k) = X(k-\delta)$ signals.
- Periodic averaging is then implemented, considering that determining the equilibrium point is important for analyzing systems.

$$X_{av}(k) = \begin{cases} \phi(k), & \exists n \in [k_0 - \Delta, k_0], \\ \dfrac{1}{\Delta} \displaystyle\sum_{i=0}^{\Delta-1} X(i+k), & \exists k > k_0, \end{cases} \tag{2}$$

  The buffer parameter Δ can be chosen arbitrarily within a specific range by trial and error at the initial stage. This value can be updated by a receptive process.

2) Poincaré Map Construction (PMC):

The use of a Poincaré map is one of the most effective approaches for the periodic solution. Thus, we implemented this concept by adding algorithms to find the Poincaré section in the 2D return map.

$$m_W^{(i)} = \frac{\displaystyle\sum_{k=i}^{i+W} (X(k) - X_{av}(k))(Y(k) - X_{av}(k))}{\displaystyle\sum_{k=i}^{i+W} (X(k) - X_{av}(k))^2}. \tag{3}$$

Using the slope of the 2-D return map (3), the change in its sign can initially be referred to in the Poincaré section. In most of the simulations, the window W was set to three samples.

3) Radius of Trajectory Calculation (RoTC), Frequency Estimation (FE), and System Damping Estimation (SDE):

Using (1) and (2), a periodic analysis environment for the time series is constructed. We can then calculate the trajectory size and estimate the frequency and damping of the oscillation using selected points.

In this study, damping is estimated with an exponential decay rate σ, rather than the relative damping ratio ζ, where ζ is defined as follows:

$$\zeta = \frac{-\sigma}{\sqrt{\sigma^2 + \omega^2}} \times 100[\%], \tag{4}$$

During the EGFE process, the mode frequency and damping are estimated at the same stage. However, equation (4) requires a known value of mode frequency ω. Therefore, this study uses a positive decay rate (negative damping) to indicate an unstable response, and vice versa.

A. TRACING TIME-VARYING MULTIPLE FREQUENCY MODES

1) TORUS AND MULTIPLE FREQUENCY MODES

While the GFE algorithm proposed in [26] detects stable cycle of oscillation, this paper extend the algorithm oscillations which has multiple frequencies. In mathematics, there are phenomenon which called invariant tori [40]. If there were stable cycle after Hopf bifurcation, this cycle can lose its stability when a pair of complex-conjugate multipliers crosses the unit circle, which are instability criteria from Floquet theory. The point where the stable cycle lose its stability called Neimark-Sacker (torus) bifurcation. Meanwhile, [41] shows a comprehensive bifurcation studies that a small sustained oscillation evolves into a torus through the Neimark-Sacker bifurcation. This paper considers this torus has multiple frequencies and construct our approach from here.

2) POINCARÉ MAP FOR TWO TORUS

This mathematical concept, which is related to two-torus dynamics presented in [34], can be applied to the existing GFE process; it was mathematically verified by [39]. In [26], the averaging system enables oscillatory behavior to decouple

the dynamic equation into two parts, as follows:

$$\begin{cases} \dot{x}_1 = f_{01}(x_1, x_2) + \varepsilon f_{11}(t, x_1, x_2, \varepsilon) \\ \dot{x}_2 = f_{02}(x_1, x_2) + \varepsilon f_{12}(t, x_1, x_2, \varepsilon). \end{cases} \tag{5}$$

where x_1, x_2 is the state variable for the specific function $f_{01}(\cdot), f_{01}(\cdot)$, which indicates the averaged function. The function $f_{11}(\cdot), f_{12}(\cdot)$ is the periodic perturbation with a boundary. Then, (5) can be interpreted as two dynamic phenomena appearing in the same system.

Therefore, this study proposes an extended approach for systems with two or more oscillatory behaviors, such as oscillations consisting of fast and slow dynamics [34]; namely, local or forced oscillations and inter-area oscillations, in power systems. We consider a problem in a system presenting torus behavior by making a canonical change of variables:

$$f = f_0(r_1, r_2, \theta_1, \theta_2) + \varepsilon f_1(r_1, r_2, \theta_1, \theta_2), \tag{6}$$

Without perturbation, ε (Fig. 1), we can define (6) as follows:

$$f = f_0(r_1, r_2, \theta_1, \theta_2), \tag{7}$$

Equation (7) aims to create a foundation for tracing and determining the multiple frequency oscillations. That is, we intend to extend the system with the oscillatory behavior of (5) to demonstrate that there are additional slow dynamics beneath the dominant dynamics. Therefore, discussions regarding specific models and observations of the torus phenomena are beyond the scope of this study. The differential equations of motion are as follows:

$$\begin{aligned} \dot{\theta}_1 &= \frac{\partial f_0}{\partial r_1} = \omega_1, \quad \dot{r}_1 = -\frac{\partial f_0}{\partial \theta_1}, \\ \dot{\theta}_2 &= \frac{\partial f_0}{\partial r_2} = \omega_2, \quad \dot{r}_2 = -\frac{\partial f_0}{\partial \theta_2}, \end{aligned} \tag{8}$$

and the solutions are $r_1 = r_{10}$ and $r_2 = r_{20}$, where ω_1 and ω_2 are constant numbers. This indicates that the motion is on a 2-torus, with radii r_1, r_2, and angles θ_1, θ_2. We define the Poincaré map on the surface of the section as follows:

$$f_0(r_1, r_2) = c, \quad \theta_2 = 0, \text{ and } mod\,(2\pi), \tag{9}$$

as shown in Fig. 1. The Poincaré mapping equations, the map of P_ε for example, are expressed as follows:

$$P_\varepsilon : (r_1, \theta_1) \to \left(r_1, \theta_1 + 2\pi \frac{\omega_1}{\omega_2}\right). \tag{10}$$

From the differential equations (8), we can easily observe that the frequencies ω_1 and ω_2 are functions of r_1 and r_2. Because $f_0(r_1, r_2) = c$, the ratio ω_1/ω_2 is a function of r_1 and constant c, which is a parameter of the mapping (10). Consequently, the mapping (10) is a twist map. Note, the time for one revolution along angle θ_2 is $T = 2\pi/\omega_2$.

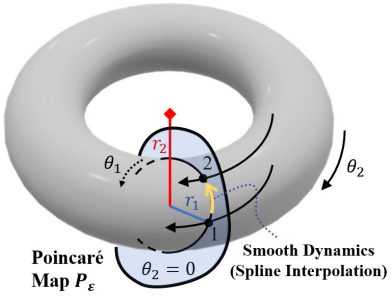

FIGURE 1. Concept of Poincaré map for two-torus phenomenon.

3) DERIVATION OF SLOW DYNAMICS

The Poincaré map $F(\cdot)$ in equation (10) is a symplectic map and is generated by the following:

$$F = r_{1,n+1}\theta_{1,n} + G_0\left(r_{1,n+1}\right), \tag{11}$$

through the relations,

$$r_{1,n} = \frac{\partial F}{\partial \theta_{1,n}}, \quad \theta_{1,n+1} = \frac{\partial F}{\partial r_{1,n+1}}, \tag{12}$$

where the function G_0 is obtained from

$$\frac{\partial G_0}{\partial r_{1,n+1}} = 2\pi \frac{\omega_1}{\omega_2} = 2\pi \frac{\partial f_0/\partial r_1}{\partial f_0/\partial r_2}. \tag{13}$$

Using the relation $f_0(r_1, r_2) = c$, we obtain the following:

$$2\pi \frac{\partial f_0/\partial r_1}{\partial f_0/\partial r_2} = g(r_1; c), \tag{14}$$

where $f(r_1; c)$ is a function of r_1 and c. Finally, we find that the function G_0 is expressed as follows:

$$G_0 = \int g(r_1; c)\, dr_1, \tag{15}$$

Apparently, the mapping of (10) has a constant c as a parameter. The mapping of (10) can be expressed in the Poincaré variables as follows:

$$X_1 = \sqrt{2r_1}\cos\theta_1 \text{ and } Y_1 = \sqrt{2r_1}\sin\theta_1, \tag{16}$$

which are also canonical variables. Therefore, the notations X_1 and Y_1 refer to the extracted oscillatory mode. The Poincaré map for the variables in (16) is shown in Fig. 1, in the space X_1Y_1, which indicates that the successive points of the mapping corresponding to the initial conditions $r_1 = r_{10}$ and $\theta_1 = \theta_{10}$ are on the circular trajectory of the constant $\sqrt{2r_1}$. The angle between the two successive points is

$$\Delta\theta_1 = 2\pi \cdot (\omega_1/\omega_2). \tag{17}$$

Note, the angle $\Delta\theta_1$ depends on r_1 (and the constant c), implying that this is a twist map. The circle with constant $\sqrt{2r_1}$ is mapped to itself; therefore, it is known as an invariant curve (circle). This invariant circle indicates the internal inter-area mode or slow dynamics of the system.

Note, (11) through (17) represent other slow dynamics of the extracted circle. Furthermore, this fact guarantees the possibility of repetitive applications of the GFE process to

monitor multiple frequency oscillations. This indicates that these derivations are not used to directly define the main algorithm, but to justify the application to the extended GFE. When r_1 is equal to zero, the system only contains one oscillatory mode. Thus, the situation is the same as that discussed in [26].

B. EXPANDED GFE PROCESS STRUCTURE

This study proposes the extended application of the GFE process to recognize multiple frequencies using time-series data.

1) CONSTRUCTION OF SMOOTH DYNAMICAL SYSTEM BY SPLINE INTERPOLATION

After the RoTC step is applied following the PMC step, the first RoT_1 value is provided with a sampling rate approximately equal to the dominant frequency f_1. This RoT_1 value is relatively sparse for defining a smooth dynamic system. Therefore, spline interpolation can be applied to this deficient dataset.

Note that the Poincaré map is given by $F(\cdot)$. Then, spline interpolation satisfies the following:

$$\left.\frac{dF_{k-1}}{dX_1}\right|_{X_{1,k}} = \left.\frac{dF_k}{dX_1}\right|_{X_{1,k}}. \tag{18}$$

This condition is also applicable to (1), considering it is quasi-continuous.

2) CORRECTIVE MEASURES AGAINST NOISE

Using (3), certain noise can be neglected because the selective PMC algorithm only considers changes in the slope. This is the primary corrective measure, considering that it guarantees error-tolerant features. In certain cases, noisy data with a magnitude exceeding that of the magnitude of the second dominant mode can affect the estimation results. Hence, an exception rule for neglecting these phase jumps while choosing the Poincaré section was implemented in the algorithm, as follows:

$$\theta_i(k) = \tan^{-1}\left(\frac{X_{av}(k) - X_1(k)}{X_{av}(k) - Y_1(k)}\right), \tag{19}$$

$$0.9 < \frac{\theta_i(k)}{\theta_i(k-1)}, \quad \frac{\theta_i(k+1)}{\theta_i(k)} < 1.1. \tag{20}$$

A flowchart is provided in Fig. 2 to present the equations used at each step to obtain the final results.

Fig. 3 presents the overall structure of the EGFE process, preceded by the primary GFE process, which is equivalent to the process introduced in [26]. Each signal processing box was applied to decompose the components from the original time-series measurement data. The tertiary GFE process is optional owing to its ambiguous result for a noisy signal. The previous method [26] focuses only on local phenomena, such as locally observed natural modes or forced oscillations. EGFEs can provide further information regarding widely spreading natural modes, which can resonate with forced oscillations. The basic concept is to extract the dynamics of

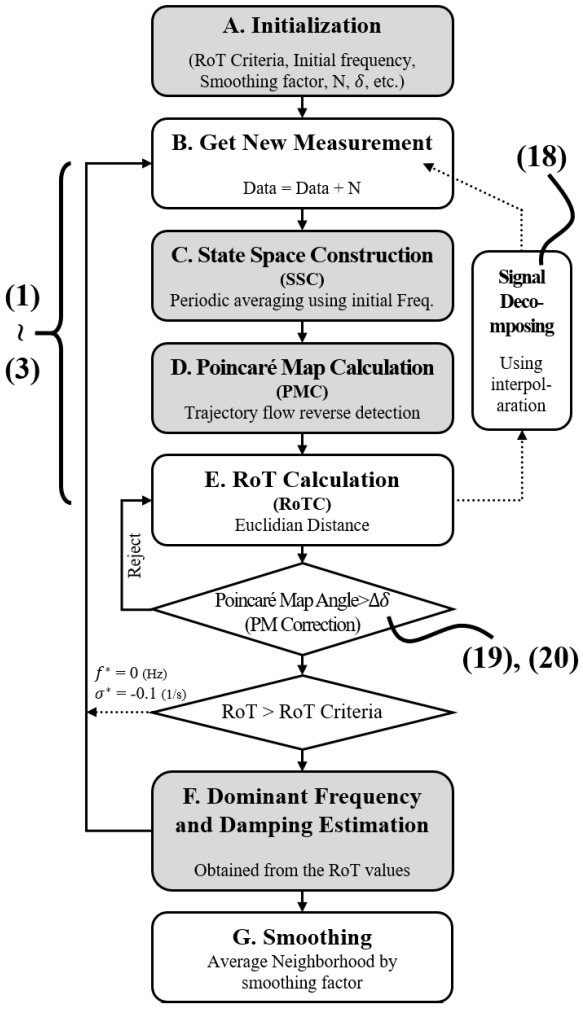

FIGURE 2. Proposed EGFE algorithm.

the RoTs or Poincaré sections by repeatedly applying the GFE method.

C. LINEAR SYSTEM APPLICATION OF EGFE PROCESS

This example presents the result of the EGFE process using an algorithm constructed, as shown in Fig. 3, based on the GFE process in [26]. Consider the power system as a simple three input and output linear system, which has a total of nine transfer functions, as shown in Fig. 4.

Among the nine transfer functions, the denominators are identical (because all areas share modes) and the numerators are unique (because individual mode shapes are different) [10]. Considering the modes, the following three dominant transfer functions are chosen: $H_1(s) = \frac{3.55}{s^2+3.55}$ for the 0.3 Hz oscillation, $H_2(s) = \frac{39.48}{s^2+39.48}$ for the 1.0 Hz oscillation, and $H_3(s) = \frac{157.75}{s^2+157.75}$ for the 2.0 Hz oscillation. The oscillation of the linear system is specified in terms of magnitude and frequency, considering the damping coefficient of each of the transfer functions is zero. Thus, the values of the damping coefficient and frequency can be chosen as the true values for an accurate and precise evaluation.

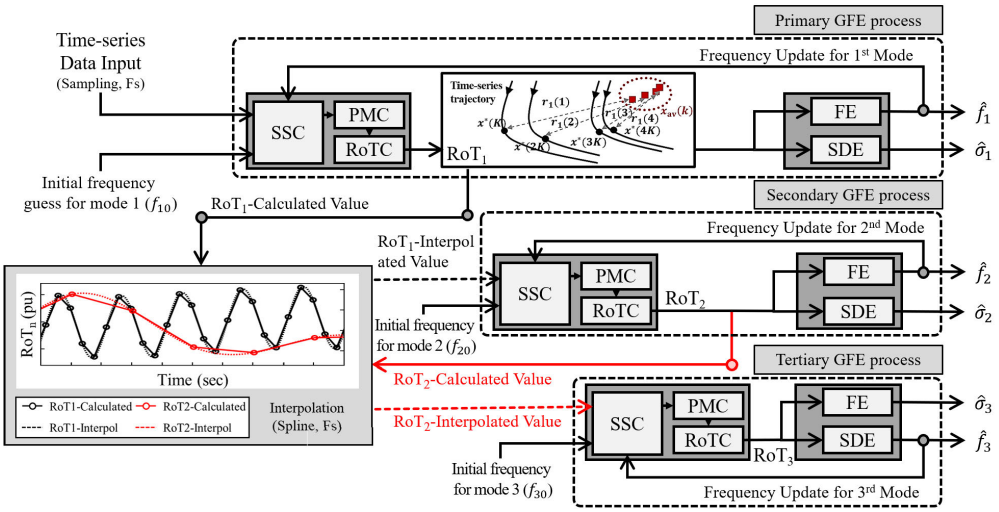

FIGURE 3. Structure of extended geometric feature extraction process for recognition of multimode frequency oscillation of power systems.

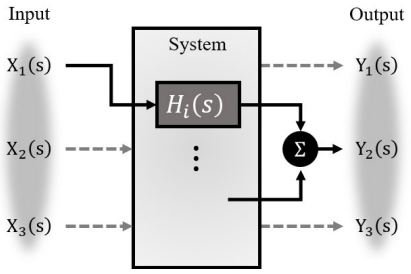

FIGURE 4. Illustration of linear system for EGFE application.

The sampling frequency F_s was set as 120 Hz without noise applied to the output, and the data consist of 12,000 samples.

1) SUMMARY OF EGFE STEPS AND THE RESULTS

With the stand-alone time-series data acquired by the linear system in Fig. 4, the RoT, damping, and frequency of each of the three components are individually estimated, as shown in Fig. 5. For Fig. 5a, the initial frequency was set falsely as 5 Hz, 0.8 Hz, and 0.15 Hz, considering that practical cases are unknown. For the other settings, the RoT criteria were set as 0.01 for only output $y(k)$. In addition, no other smoothing factor was applied to this noiseless case. Fig. 5b presents the result of the state space construction and Poincaré Map Calculation. Despite the initial frequency being incorrect, the circular trajectory was detected for every three components of the output.

Fig. 5c presents the normalized frequency spectrum of the signal and the results of the RoT for the secondary and tertiary GFE processes. The original signal has the following three components: 2, 1, and 0.3 Hz. After the primary stage, the dominant 2 Hz component disappears, and the 1 Hz component appears as the dominant component. Finally, the 0.3 Hz component remains in the tertiary stage. Note, this 0.3 Hz component appears to have a magnitude of approximately 0.1 without normalization of the spectrum, and it retains the mode information; however, its actual magnitude is significantly smaller (mean value of 0.0025). Fig. 5d presents the frequency plane of the three estimated components for damping and frequency. The real axis value (related to damping) fluctuates owing to the perturbation at 5 s to 5.1 s. The performance of damping and the frequency results are discussed in the following section.

D. PERFORMANCE MEASURE OF EGFE

To perform an accuracy test for EGFE, a comparison between the actual and practical output is necessary. Therefore, a simple signal with three exponential components is adopted only in this section, by changing the damping σ_i and frequency f_i in the equation form of (21).

$$x[k] = \sum_{i=1}^{3} A_i e^{\sigma_i \cdot kT_s} \cdot \cos(2\pi f_i \cdot kT_s + \varphi_i), \tag{21}$$

1) MULTI-CLASS CONFUSION MATRIX

For the performance evaluation, the accuracy and F1 score are the main considerations. To manage the F1 score, it is necessary to determine the precision and recall. Thus, the input data for each time interval are applied equally for each process. Basic factors, such as true positive (TP), true negative (TN), false positive (FP), and false negative (FN) are used to examine these concepts [42]. These factors can be directly calculated using the confusion matrix presented in Table 1. Because the EGFE process uses balanced data, the accuracy is suitable for performance evaluation. Accuracy is defined as shown in (22).

$$(Accuracy) = \frac{\sum_{j=1}^{n} x_{jj}}{\sum_{j=1}^{n} \sum_{i=1}^{n} x_{ij}} \tag{22}$$

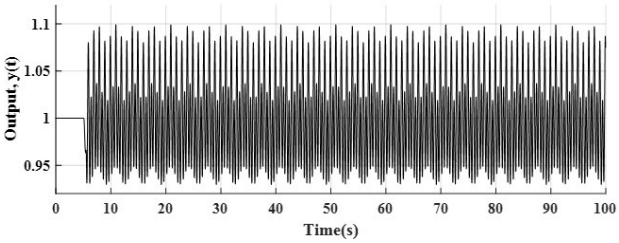

(a) Output acquired after Initialization (step A) and new measurement (step B).

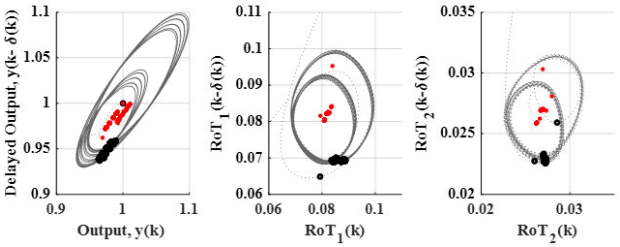

(b) Results of SSC (step C) and PMC (step D) from output $y(k)$ to $RoT_2(k)$.

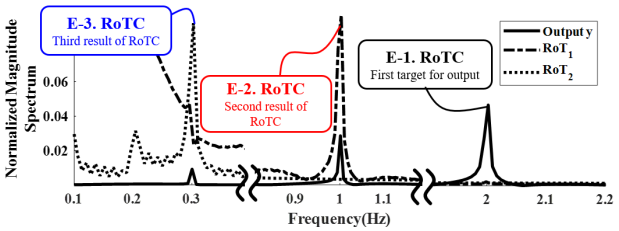

(c) Spectrum analysis for the result of RoTC (step E) for output $y(k)$, RoT_1 and RoT_2.

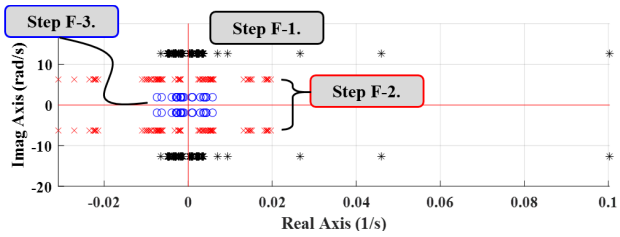

(d) Representation of three modes after applying frequency and damping estimation (step F).

FIGURE 5. Multifrequency oscillation recognition for the three components of the linear system output.

TABLE 1. Confusion matrix with *N* classes.

		Classified Number			
		Class 1	Class 2	...	Class n
Actual Number	Class 1	x_{11}	x_{12}	$\cdots$	x_{1n}
	Class 2	x_{21}	x_{22}	$\cdots$	x_{2n}
	$\vdots$	$\vdots$	$\vdots$	$\ddots$	$\vdots$
,	Class n	x_{n1}	x_{n2}	$\cdots$	x_{nn}

TABLE 2. Classification of estimated damping and frequency.

	Damping Estimation	Frequency Estimation
Class 1	$\hat{\sigma}_i < -2\%$	$\hat{f}_i < (1-2\varepsilon)f_i$
Class 2	$-2\% < \hat{\sigma}_i < -1\%$	$(1-2\varepsilon)f_i < \hat{f}_i < (1-\varepsilon)f_i$
Class 3	$-1\% < \hat{\sigma}_i < 1\%$	$(1-\varepsilon)f_i < \hat{f}_i < (1+\varepsilon)f_i$
Class 4	$1\% < \hat{\sigma}_i < 2\%$	$(1+\varepsilon)f_i < \hat{f}_i < (1+2\varepsilon)f_i$
Class 5	$2\% < \hat{\sigma}_i$	$(1+2\varepsilon)f_i < \hat{f}_i$

2) PROBLEM FORMULATION FOR ACCURACY TEST OF EGFE

In [43] and [44], the acceptable damping limit is system-dependent and typically in the range of 3%—5%, which is a significantly large criterion for a long-term evaluation sample. These damping criteria are defined in a small-signal stability assessment, which is subject to the low-frequency oscillation condition. Therefore, the damping criterion for the accuracy and error analysis of this simple example of a waveform was chosen as −2%–2% to avoid extreme conditions. Consequently, the class for damping and frequency estimation was chosen as shown in Table 2.

After the primary and secondary GFE processes, the damping estimation has accuracies of 92.98% and 98.27%, respectively. Meanwhile, the tertiary GFE process has an overall accuracy of 57.83% (F1 score is 60.72%), which indicates a poor performance when compared to the other components. Regardless, the recall and precision of the positive damping case are relatively higher than those of the negative damping case, which indicates that the tertiary GFE process works sufficiently on unstable low-frequency oscillations. In contrast, the frequency estimation performance demonstrates an accuracy exceeding 95% for all three components at $\varepsilon = 10\%$, where ε refers to the range of confidence of the frequency estimation.

We added this performance test only for this simple waveform application, considering the known true values for damping and frequency. Thus, the validations presented in the following sections are only concerned with the existing signal processing methods, such as the Prony method.

III. CASE STUDY ON WECC 179 BUS POWER SYSTEM

A. SYSTEM DESCRIPTION

Fig. 6a presents area 1 of the Western Electricity Coordinating Council (WECC) 179 bus system. The damping coefficients (D_i) of generators 6, 11, and 79 are 3.0, −8.0, and 0, respectively, whereas those of the other generators are equal to 4.0. The round rotor generator model, GENROU, was used for generators 6 and 79, and the constant internal voltage generator model GENCLS was applied for the other generators. All loads were assumed to conform to the constant MVA model. The forced signal input shown in Fig. 6b was injected into the excitation system with a frequency of 1.0 Hz at generator 79.

1) PRELIMINARY STUDY USING SMALL-SIGNAL ANALYSIS

The outcome of the small-signal analysis indicates two inter-area modes. The first mode has a real value of −0.0158 1/s and an imaginary value of 2.8711 rad/s with a

TABLE 3. Description of measurement location and comparison results of EGFE and prony method.

Measurement Number (M#)	Branch Location (Bus No. Bus Name)	RoT-Proposed EGFE Method -Maximum Values at 200s (1/s)		Magnitude-Prony Method -Maximum Values at 200s (1/s)		Distance from FO Source (Level)	Distance from NO Source (Level)
		1.0 (Hz)	0.433 (Hz)	1.0 (Hz)	0.433 (Hz)		
M1	34 CA230 - 35 CMAINGM	0.427	0.233	0.155	0.142	4	20
M2	31 CANADA - 30 CANADG1	3.285	0.114	1.667	0.094	2	17
M3	80 NORTH - 79 NORTHG3	10.028	0.347	5.130	0.190	0	16
M4	80 NORTH - 78 HANFORD	3.674	0.131	1.892	0.109	1	15
M5	66 MONTANA - 65 MONTAG1	0.170	0.283	0.166	0.189	2	16
M6	76 JOHNDAY - 77 JOHNDAY	9.497	0.225	4.833	0.106	3	14
M7	82 GRIZZLY - 76 JOHNDAY	2.232	0.226	1.172	0.138	3	13
M8	85 MIDPOINT - 36 BRIDGER2	0.671	0.073	0.374	0.057	12	5
M9	158 EMERY - 159 EMERY	0.246	0.202	0.115	0.153	16	4
M10	5 CRAIG - 11 HAYDEN	Non-observable	0.500	0.028	0.434	16	0
M11	8 FOURCORN - 9 FCNGN4CC	Non-observable	0.226	0.043	0.138	18	3

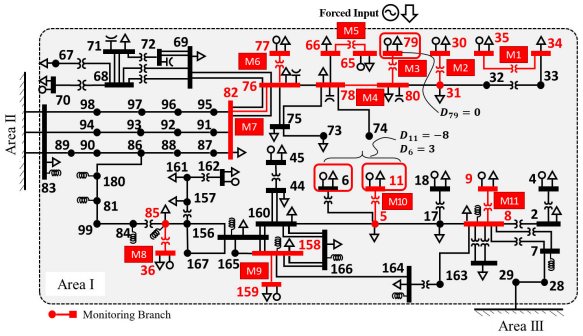

(a) WECC 179 bus power system configuration. Forced input was applied to the generator excitation system of the generator at bus 79.

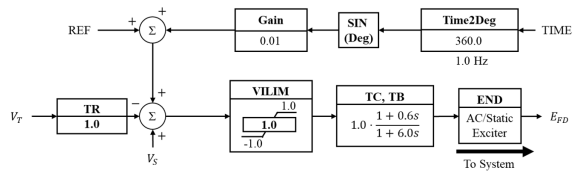

(b) Forced input with a frequency of 1.0 Hz was applied to the exciter of generator 79.

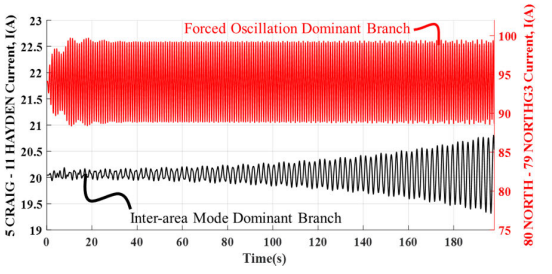

(c) Current response for forced and natural oscillations.

FIGURE 6. WECC 179 bus power system and the forced and natural oscillations.

mode frequency of 0.457 Hz and damping of 0.55%. The second mode has a real value of −0.029 1/s and an imaginary value of 4.361 rad/s with a mode frequency of 0.6941 Hz and damping of 0.67%. The participation factors for the first mode are 1.0, 0.52, and 0.5 for generators 11, 6, and 45, respectively. The second-mode participation factors are 1.0, 0.48, 0.44, and 0.35 for generators 11, 6, 45, and 9, respectively. Therefore, the dominant state for the two modes is the speed of generator 11.

The system damping for both modes is positive and stable. The gain of the external force is adjusted to have the largest peak-to-peak value among the active outputs of all generators at approximately 80 MW at generator 79. Regardless, the output increases to 419 MW over time, owing to the resonance with the first natural mode.

2) TIME AND FREQUENCY DOMAIN OBSERVATIONS

From here, we use current response to detect the oscillation, while the KEPCO operators practically use branch quantities for oscillation analysis. Fig. 6c presents the current response of generator 79 over 200 s. For the measurement branch of M3, from bus 80 to bus 79, forced oscillation is dominant. Furthermore, for the measurement branch of M10, from bus 5 to bus 11, the natural mode of 0.433 Hz is dominant. The overall observations from comparing the Prony analysis are provided in Table 3. Both the RoT of EGFE and Prony magnitudes are similar; both are relative to the distance between the forced and natural oscillation sources.

Fig. 7 illustrates the frequency spectrum for the current measured from M1 to M11, in which M10 and M11 present the largest magnitude at 0.46 Hz of the inter-area mode. Branches M2 to M7 show a large magnitude at 1 Hz of the forced oscillation. However, measurement branch M3 does not have the largest magnitude because its steady-state or 0 Hz magnitude for the current is up to 94 pu. The forced response is the largest at branches M6 and M7. The results of the EGFE process are discussed in the next section.

B. EVALUATION OF MULTIPLE FREQUENCY OSCILLATION BASED ON EGFE RESULTS

This section focuses on the EGFE results for the 0.46 Hz mode, which covers most locations in the area of interest. This inter-area natural oscillation triggered by the forced input involves many generators operating in the mode, thus requiring comprehensive observation. In this case, the appropriate

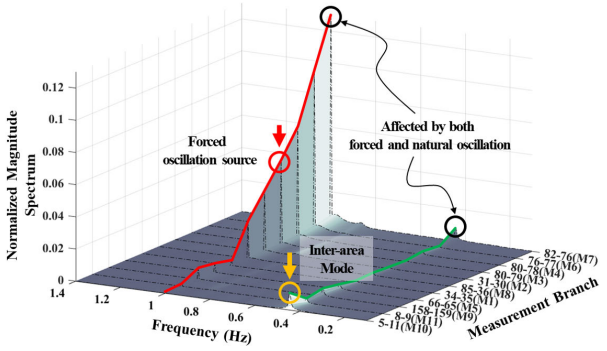

FIGURE 7. Normalized magnitude spectrum for WECC 179 bus power system. The oscillation was observed as a forced response and inter-area mode.

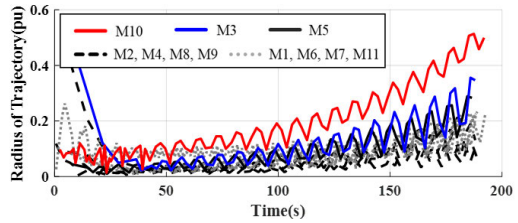

(a) Radius of trajectory for area 1 in WECC 179 bus benchmark system.

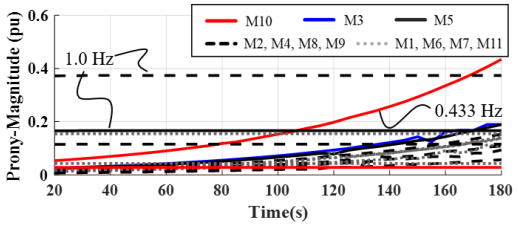

(b) Magnitude in Prony method for validation.

FIGURE 8. Comparison between amplitudes obtained via the proposed method and Prony method for the inter-area mode with a 0.433 Hz oscillation.

strategy is typically to detect fluctuations in the power flows or currents along the oscillation path; thus, the largest RoTs of the oscillations in the network can no longer be used as an indication of the source location.

1) RADIUS OF TRAJECTORY PROFILE ASSESSMENT

Fig. 8a presents the RoT for all measured branches. Fig. 8b presents the magnitude estimated by using the Prony method. M9, which monitors the current in the branch between buses 5 and 7, indicates the largest RoT, considering it is closest to the generator unit that has negative damping parameter settings. The decomposed RoT obtained from the secondary GFE at branch M3 was the highest, followed by that at M9. Moreover, the RoTs for the remaining measurement locations are comparatively smaller because they are located between the two natural and forced oscillation sources.

2) ESTIMATION OF SYSTEM DAMPING AND FREQUENCY

After applying the EGFE for all measured branches, the measurement locations near generators 79 and 11 present clear and similar results, as depicted in Fig. 9a and Fig. 9c. These results were also compared to the Prony method results in Fig. 9b and Fig. 9d.

Fig. 9a shows the estimated system damping for the selected branches. Most of the selected locations indicate a damping of approximately 0.013. Similar Prony damping results can be observed in Fig. 9b. Therefore, the damping trend in this case indicates unstable responses with large RoT values at most locations. Note, the damping in the EGFE results could differ from that obtained from the small-signal analysis, which is calculated using the linear form at the equilibrium point.

Furthermore, the proposed result indicates that the detected time is different for each branch location owing to the RoT criteria. However, the response comprising both natural and forced inputs in this case continuously changes and can lead to significantly more serious situations.

Fig. 9c presents the calculated frequency for the selected branch quantities. Similarly, the frequencies calculated at M3 and M10, which are near the inter-area oscillation source, are accurately estimated at 0.43 Hz. Every location, except for M1, presents sufficiently large frequency results that can be applied to the EGFE process. In contrast, measurement branch M1 has changing frequency values, which makes it difficult to apply the frequency results owing to its low magnitude composition for both forced and natural modes. This is also the case with the damping estimation. Furthermore, measurement location M7, which monitors the branch between buses 82 and 76, yields the best estimation result for both forced and natural oscillations.

IV. KEPCO SYSTEM OSCILLATION EVENT RECORDED WITH PMU

A. SYSTEM AND EVENT DESCRIPTION

Fig. 10 presents the system configuration for the oscillation event that occurred in the KEPCO system, which measure the current and voltage information through PMU monitoring at 23 locations for the 345-kV system and two locations for the 765-kV system in the metropolitan, western, and eastern coastal areas. The oscillation event was observed on November 22, 2019. The data were recorded for 2 h (UTC, 15:00:00–17:01:30) at the eastern area. Table 4 summarizes the branch locations and their current and MW flows under normal conditions. The PMU in the eastern area (connected to DH#1,2 buses) collected data at a rate of 120 samples/s, considering both bus and line quantities for the magnitude and angle of frequency. The PMU monitored the branch values of the phase current and angle with active and reactive power.

The oscillation event was triggered during the scheduled commissioning of the new TCSC facility installed between the DH and SJC buses, the two branches of B5 and B6. Specifically, owing to the operation mode of the TCSC, a forced response of approximately 2 Hz was observed in the local area. Furthermore, as indicated in the previous section, inter-area mode oscillation was also found in the

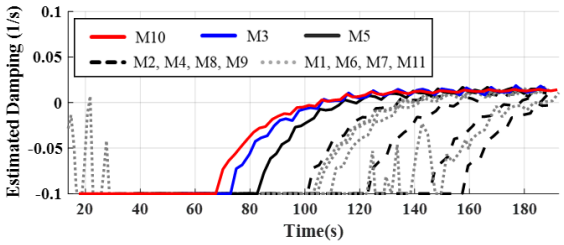

(a) Estimated damping at measurement locations for natural modes of 0.433 Hz. Most branches present similar damping in the presence of a forced oscillation.

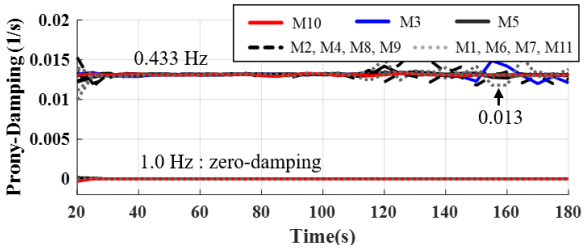

(b) Validation by Prony method. Calculated damping is shown at measurement locations for natural modes of 0.433 Hz and a forced oscillation of 1.0 Hz.

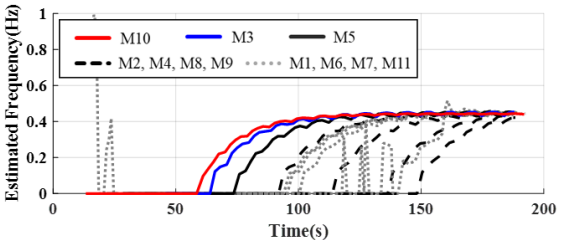

(c) Estimated frequency at measurement locations for natural modes of 0.433 Hz. Most branches present similar damping, including for the forced input.

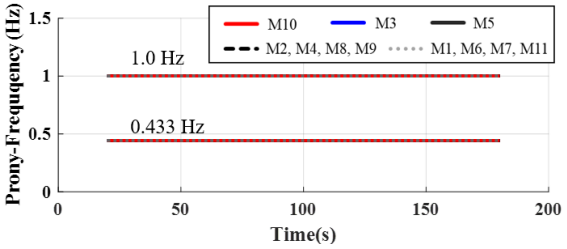

(d) Validation by Prony method. The selected frequency is shown at the measurement locations for natural modes of 0.433 Hz and a forced oscillation of 1.0 Hz.

FIGURE 9. Time-varying mode tracking for multifrequency oscillation in the WECC 179 bus power systems.

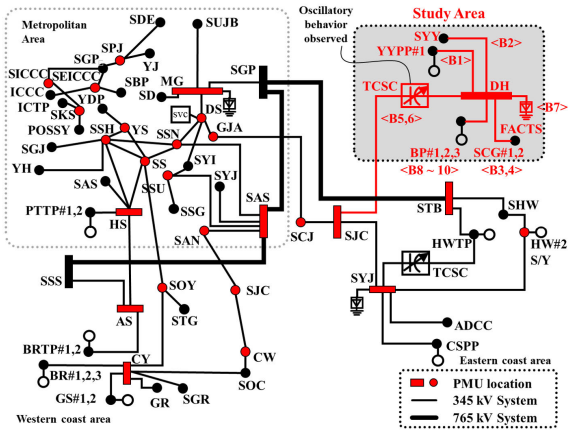

FIGURE 10. Configuration of KEPCO systems. The oscillation event was observed as the local mode and inter-area mode.

measurement data. Fig. 11 presents the MW flow measured at each location, where the current measurements were used for EGFE application. Fig. 12a presents the current measurement data for the branches connected to buses DH#1 and DH#2. The peak-to-peak value of the active power during the third interval of 1,050 s was 15 MW from 2019-11-22, 15:30:35 to 2019-11-22, 15:48:20. The peak-to-peak active power during the final 760 s was 50 MW, which was observed from 2019-11-22, 16:36:50, to 2019-11-22, 16:49:30. The TCSCs were bypassed after experiencing four incidents. The results obtained by applying the fast Fourier transform (FFT) differed from the time interval; however, the overall dominant frequency was 2.14 Hz. In contrast, the FFT shows that the other low-frequency components were approximately 1.0 and

TABLE 4. Description of PMU measurement locations and branch quantities in normal conditions.

No.	From Bus	To Bus	Normal Condition	
			Current (A)	P Flow (MW)
B1	DH#1	YYPP#1	178.30	73.7
B2	DH#1	SYY	184.08	80.3
B3	DH#1	SCG#1	805.66	-494.8
B4	DH#1	SCG#2	811.67	-495.2
B5	DH#2	SJC#1	869.49	535.0
B6	DH#2	SJC#2	862.88	538.7
B7	DH#2	FACTS	498.68	2.5
B8	DH#2	BP#1	559.60	-344.2
B9	DH#2	BP#2	562.32	-342.8
B10	DH#2	BP#3	546.77	-337.1

0.1 Hz. These results are discussed in the next section, which relates to the EGFE evaluation for the branch between buses DH#2 and SJC#1 (B5), which is where the main phenomenon was observed.

B. EVALUATION OF MULTIPLE FREQUENCY OSCILLATION USING EGFE RESULTS OF ACTUAL PMU DATA

Fig. 12b presents the RoT values for the dominant to low-frequency modes. The RoT slowly decreases between 0 and 300 s and 300 and 600 s; spikes can be observed at modes 2 and 3 owing to the interpolation error.

Figs. 13a and 13b present the estimated system damping and frequency for the three modes extracted using the EGFE process. The system is in a critical situation if only the estimated damping is considered for the three modes. However, the RoTs for the lower frequency modes are relatively smaller than those of the local oscillation mode. Therefore, in this

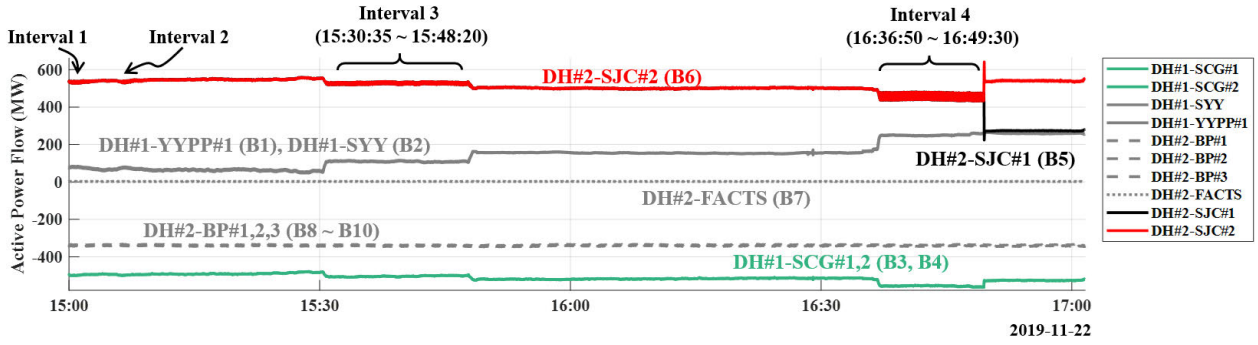

FIGURE 11. MW flow measured in each location. The main oscillations were observed at B5 and B6.

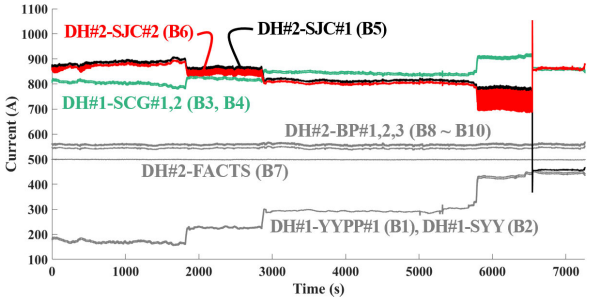

(a) Current measured near the oscillation source where the TCSCs are installed.

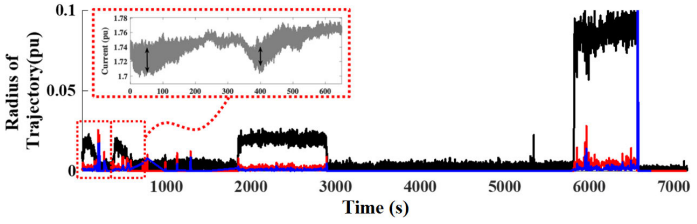

(b) Radius of trajectory for the three components of the signal.

FIGURE 12. Measurement data acquired from the nearby oscillation source in the eastern area of KEPCO system.

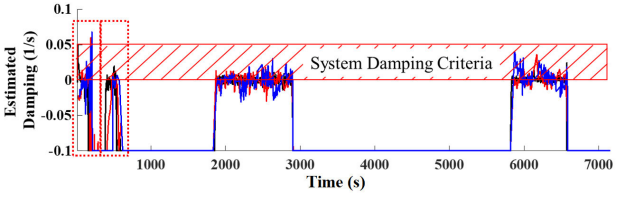

(a) Estimated damping for the three components of the current signal.

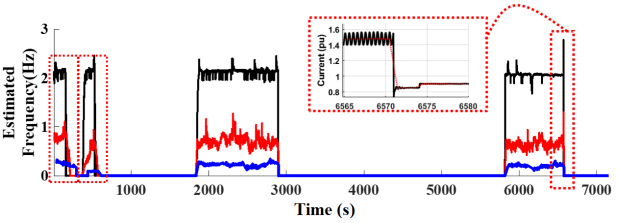

(b) Estimated frequency for the three components of the signal.

FIGURE 13. Time-varying mode tracking in the eastern area of KEPCO system.

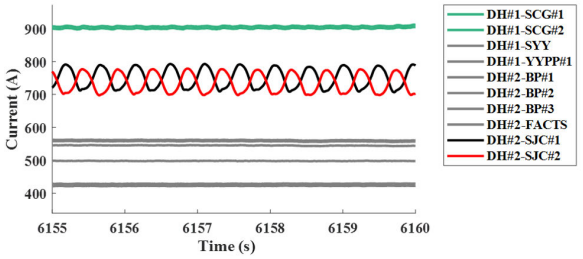

(a) Oscillation observed from current measured at DH#2-SJC#1(B5) and DH#2-SJC#2(B6). The oscillations have opposite phases.

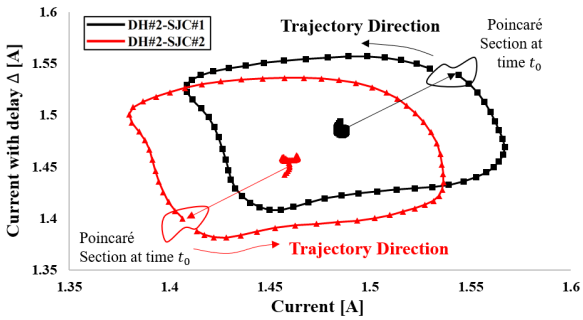

(b) Constructed trajectories for DH#2-SJC#1(B5) and DH#2-SJC#2(B6). The Poincaré map is formed at the opposite location.

FIGURE 14. Detailed observation over 5 s at branches DH#2-SJC#1(B5) and DH#2-SJC#2(B6).

case, the incident did not cause further harm to the KEPCO system because the wide-area modes had a significantly small impact. Similarly, Prony analysis was applied, having an order model of 200 and data length of 700. The Prony analysis results for the time interval ranging from 6,014 to 6,020 s yield the following two observable modes: (i) a mode with 39 pu amplitude, 0.0034 1/s damping, and 2.1 Hz frequency and (ii) a mode with 10 pu amplitude, −1.5 1/s damping, and 0.78 Hz frequency. Note, Prony analysis preserves more information upon comparing RoT to that of the EGFE result.

Meanwhile, the oscillation observed in the branch from bus DH#2 to SJC#1 (B5) shows a phase opposite to that of the branch from bus DH#2 to SJC#2 (B6). Fig. 14a presents the current measurement for the time interval from 6,155 s to 6,160 s, where the responses of DH#2 to SJC#1 (B5) and SJC#2(B6) clearly have opposite phases. Fig. 14b shows the mapping of the current measurement and its delayed value for the same time interval. The measurement data clearly indicates that the two locations have opposite end points. Therefore, the oscillation is caused by the operating condition of the TCSC controller; however, paradoxically, it is not widely spread by the other TCSC controller and disappears within the local area. The opposite cases for oscillations which are precursor to power system swing instabilities are provided in [45].

Moreover, there are growing concerns of renewable or inverter-based resources integration from the perspective of power system dynamics and stability. But, some recent researches proposes some control strategies that, with appropriate control in renewables, the oscillation phenomenon can rather be suppressed [46].

V. CONCLUSION

In this study, an extended application of the GFE was proposed to determine and trace time-varying modes associated with multiple frequency oscillations based on power system measurement data. The most important contribution of the study is that the proposed method determines multiple internal system modes, whereas the existing time-series based approaches focus on the dominant components. Further, tracing the time-varying modes and comparing them with the dominant component enable the operator to determine the severity of the oscillation effect on the system. Finally, the operator can determine when to apply the control scheme based on the geometrical information provided by the EGFE process by calculating the frequency at each measurement location.

There were practical challenging issues in the implementation stage, such as process disruption, considering that the desired output of the EGFE algorithm has unstructured oscillation features, whereas the input has a structured form with uniformly sampled measurements. Therefore, for future studies related to time-series-based multifrequency, enhancing the adaptability or flexibility of the algorithm is recommended by considering the computational burden of each categorized stage.

REFERENCES

[1] *Reliability Guideline: Forced Oscillation Monitoring & Mitigation*, North Amer. Electr. Reliabilty Corp., Atlanta, GA, USA, Sep. 2017. [Online]. Available: https://www.nerc.com/comm/PC_Reliability_Guidelines_DL/Reliability_Guideline_-_Forced_Oscillations_-_2017-07-31_-_FINAL.pdf

[2] S. A. N. Sarmadi and V. Venkatasubramanian, "Inter-area resonance in power systems from forced oscillations," *IEEE Trans. Power Syst.*, vol. 31, no. 1, pp. 378–386, Jan. 2016.

[3] R. Xie and D. Trudnowski, "Distinguishing features of natural and forced oscillations," in *Proc. IEEE Power Energy Soc. Gen. Meeting*, Jul. 2015, pp. 1–5.

[4] J. Liu, W. Yao, J. Wen, H. He, and X. Zheng, "Active power oscillation property classification of electric power systems based on SVM," *J. Appl. Math.*, vol. 2014, pp. 1–9, May 2014.

[5] S. Nuthalapati, *Power System Grid Operation Using Synchrophasor Technology*. New York, NY, USA: Springer, 2019.

[6] R. B. Myers and D. J. Trudnowski, "Effects of forced oscillations on spectral-based mode-shape estimation," in *Proc. IEEE Power Energy Soc. Gen. Meeting*, Jul. 2013, pp. 1–6.

[7] Y. Gao, D.-C. Liu, G.-B. Huang, and Q.-Y. Shi, "Locating method of disturbance source of forced power oscillation based on prony anyasis," in *Proc. China Int. Conf. Electr. Distrib.*, Sep. 2012, pp. 1–4.

[8] V. Jain, S. T. Nagarajan, and R. Garg, "Study of forced oscillations in two area power system," in *Proc. 2nd IEEE Int. Conf. Power Electron., Intell. Control Energy Syst. (ICPEICES)*, Oct. 2018, pp. 96–101.

[9] D. S. Laila, A. R. Messina, and B. C. Pal, "A refined Hilbert–Huang transform with applications to inter-area oscillation monitoring," in *Proc. IEEE Power Energy Soc. Gen. Meeting*, Jul. 2009, p. 1.

[10] A. R. Messina, V. Vittal, G. T. Heydt, and T. J. Browne, "Nonstationary approaches to trend identification and denoising of measured power system oscillations," *IEEE Trans. Power Syst.*, vol. 24, no. 4, pp. 1798–1807, Nov. 2009.

[11] M. Ghorbaniparvar, "Survey on forced oscillations in power system," *J. Mod. Power Syst. Clean Energy*, vol. 5, no. 5, pp. 671–682, Jun. 2017.

[12] J. D. Follum, F. K. Tuffner, L. A. Dosiek, and J. W. Pierre, "Power system oscillatory behaviors: Sources, characteristics, & analyses," Pacific Northwest Nat. Lab., Richland, WA, USA, Tech. Rep. PNNL-26375, May 2017.

[13] N. Zhou, "A coherence method for detecting and analyzing oscillations," in *Proc. IEEE Power Energy Soc. Gen. Meeting*, Jul. 2013, pp. 1–5.

[14] M. Donnelly, D. Trudnowski, J. Colwell, J. Pierre, and L. Dosiek, "RMS-energy filter design for real-time oscillation detection," in *Proc. IEEE Power Energy Soc. Gen. Meeting*, Jul. 2015, pp. 1–5.

[15] F. Zhang, L. Cheng, W. Gao, and R. Huang, "Synchrophasors-based identification for subsynchronous oscillations in power systems," *IEEE Trans. Smart Grid*, vol. 10, no. 2, pp. 2224–2233, Mar. 2019.

[16] H. Cho, S. Oh, S. Nam, and B. Lee, "Non-linear dynamics based subsynchronous resonance index by using power system measurement data," *IET Gener., Transmiss. Distrib.*, vol. 12, no. 17, pp. 4026–4033, Sep. 2018.

[17] G. Chavan, M. Weiss, A. Chakrabortty, S. Bhattacharya, A. Salazar, and F.-H. Ashrafi, "Identification and predictive analysis of a multi-area WECC power system model using synchrophasors," *IEEE Trans. Smart Grid*, vol. 8, no. 4, pp. 1977–1986, Jul. 2017.

[18] *Oscillation Event 03.12.2017: System Protection and Dynamics WG*, ENTSO-E, Brussels, Belgium, Mar. 2018. [Online]. Available: https://www.entsoe.eu/Documents/SOC%20documents/Regional_Groups_Continental_Europe/OSCILLATION_REPORT_SPD.pdf

[19] P. Korba, M. Larsson, and C. Rehtanz, "Detection of oscillations in power systems using Kalman filtering techniques," in *Proc. IEEE Conf. Control Appl. (CCA)*, vol. 1, Jun. 2003, pp. 183–188.

[20] P. Korba, "Real-time monitoring of electromechanical oscillations in power systems: First findings," *IET Gener., Transmiss. Distrib.*, vol. 1, no. 1, pp. 80–88, 2007.

[21] P. Korba and K. Uhlen, "Wide-area monitoring of electromechanical oscillations in the nordic power system: Practical experience," *IET Gener., Transmiss. Distrib.*, vol. 4, no. 10, pp. 1116–1126, 2010.

[22] M. Maurer, F. Gutekunst, and G. Scheffknecht, "Dynamic parameter estimation of inter-area oscillations in a power system by a combination of Kalman-filtering and wavelet transformation techniques," *IFAC Proc. Volumes*, vol. 47, no. 3, pp. 8196–8201, 2014. [Online]. Available: http://www.sciencedirect.com/science/article/pii/S147466701642906X

[23] J. Turunen, "A wavelet-based method for estimating damping in power systems," Ph.D. dissertation, Aalto Univ., Espoo, Finland, 2011. [Online]. Available: http://urn.fi/URN:ISBN:978-952-60-4051-6

[24] B. Panomruttanarug and R. Longman, "The advantages and disadvantages of Kalman filtering in iterative learning control," in *Proc. AAS/AIAA Space Flight Mech. Meeting*, vol. 130, Jan. 2008, pp. 347–365.

[25] U. Agrawal, J. Follum, J. W. Pierre, and D. Duan, "Electromechanical mode estimation in the presence of periodic forced oscillations," *IEEE Trans. Power Syst.*, vol. 34, no. 2, pp. 1579–1588, Mar. 2019.

[26] H. Cho, N. Choi, and B. Lee, "Oscillation recognition using a geometric feature extraction process based on periodic time-series approximation," *IEEE Access*, vol. 8, pp. 34375–34386, 2020.

[27] M. A. Khan and J. W. Pierre, "Detection of periodic forced oscillations in power systems using multitaper approach," *IEEE Trans. Power Syst.*, vol. 34, no. 2, pp. 1086–1094, Mar. 2019.

[28] U. Agrawal and J. W. Pierre, "Detection of periodic forced oscillations in power systems incorporating harmonic information," *IEEE Trans. Power Syst.*, vol. 34, no. 1, pp. 782–790, Jan. 2019.
[29] J. Follum and J. W. Pierre, "Detection of periodic forced oscillations in power systems," *IEEE Trans. Power Syst.*, vol. 31, no. 3, pp. 2423–2433, May 2016.
[30] N. Zhou and J. Dagle, "Initial results in using a self-coherence method for detecting sustained oscillations," *IEEE Trans. Power Syst.*, vol. 30, no. 1, pp. 522–530, Jan. 2015.
[31] N. Zhou, "A cross-coherence method for detecting oscillations," *IEEE Trans. Power Syst.*, vol. 31, no. 1, pp. 623–631, Jan. 2016.
[32] H. Ye, Y. Liu, P. Zhang, and Z. Du, "Analysis and detection of forced oscillation in power system," *IEEE Trans. Power Syst.*, vol. 32, no. 2, pp. 1149–1160, Mar. 2017.
[33] Y. Chi, B. Tang, J. Hu, X. Tian, H. Tang, Y. Li, S. Sun, L. Shi, and L. Shuai, "Overview of mechanism and mitigation measures on multi-frequency oscillation caused by large-scale integration of wind power," *CSEE J. Power Energy Syst.*, vol. 5, no. 4, pp. 433–443, 2019.
[34] J. D. Hadjidemetriou, "The Poincaré map and the method of averaging: A comparative study," *Nonlinear Phenomena Complex Syst.*, vol. 11, no. 2, pp. 149–157, 2008.
[35] R. Seydel, *Practical Bifurcation and Stability Analysis*, vol. 5. Berlin, Germany: Springer, 2009.
[36] V. Ajjarapu and B. Lee, "Bifurcation theory and its application to nonlinear dynamical phenomena in an electrical power system," *IEEE Trans. Power Syst.*, vol. 7, no. 1, pp. 424–431, Feb. 1992.
[37] J. Devadason, P. Moses, and W. Fei, "Bifurcation analysis of weak electrical grids considering different load representations," in *Proc. IEEE 7th Int. Conf. Smart Energy Grid Eng. (SEGE)*, Aug. 2019, pp. 208–212.
[38] S. Maslennikov and E. Litvinov, "ISO new england experience in locating the source of oscillations online," *IEEE Trans. Power Syst.*, vol. 36, no. 1, pp. 495–503, Jan. 2021.
[39] H. K. Khalil and J. W. Grizzle, *Nonlinear Systems*, vol. 3. Upper Saddle River, NJ, USA: Prentice-Hall, 2002.
[40] Y. A. Kuznetsov, *Elements of Applied Bifurcation Theory*, 2nd ed. Berlin, Germany: Springer-Verlag, 1998.
[41] D. Wu, P. Vorobev, S. C. Chevalier, and K. Turitsyn, "Modulated oscillations of synchronous machine nonlinear dynamics with saturation," *IEEE Trans. Power Syst.*, vol. 35, no. 4, pp. 2915–2925, Jul. 2020.
[42] A. Tharwat, "Classification assessment methods," *Appl. Comput. Informat.*, vol. 17, no. 1, pp. 168–192, Jan. 2021.
[43] P. Kundur, N. J. Balu, and M. G. Lauby, *Power System Stability and Control*, vol. 7. New York, NY, USA: McGraw-Hill, 1994.
[44] U. Kerin, E. Lerch, and G. Bizjak, "Monitoring and reporting of security of power system low-frequency oscillations," *Electr. Power Compon. Syst.*, vol. 38, no. 9, pp. 1047–1060, 2010, doi: 10.1080/15325001003649450.
[45] Y. Susuki and I. Mezic, "Nonlinear koopman modes and a precursor to power system swing instabilities," *IEEE Trans. Power Syst.*, vol. 27, no. 3, pp. 1182–1191, Aug. 2012.
[46] T. Sadamoto, A. Chakrabortty, T. Ishizaki, and J.-I. Imura, "Retrofit control of wind-integrated power systems," *IEEE Trans. Power Syst.*, vol. 33, no. 3, pp. 2804–2815, May 2018.

HWANHEE CHO (Member, IEEE) received the B.S. degree from Dankook University, Yongin, in 2014, and the Ph.D. degree from Korea University, Seoul, in 2020. Since 2020, he has been a Senior Researcher with the Korea Railroad Research Institute (KRRI). His research interests include power system stability, nonlinear systems, power system measurements for wide-area monitoring systems, and power system oscillation.

NAMKI CHOI (Graduate Student Member, IEEE) received the B.S. degree from Korea University, Seoul, in 2018, where he is currently pursuing the Ph.D. degree in electrical engineering and electronics. His research interests include power system analysis and studies regarding the effect of inverter-based resources, specifically interactions between renewable energy systems (wind and PV, among others), and power systems.

SUCHUL NAM (Member, IEEE) received the B.S. and M.S. degrees in electrical engineering from Korea University, Seoul, Republic of Korea, in 2001 and 2006, respectively. Since 2006, he has been with the Next Generation Transmission Substation Laboratory, KEPCO Research Institute, Daejeon, Republic of Korea. His research interests include power system operation, stability and control, PMU applications, and real-time dynamic simulation.

BYONGJUN LEE (Senior Member, IEEE) is currently a Professor with the School of Electrical Engineering, Korea University. His research interest includes span power system planning and operation. His work focuses on the improvement of power system stability, mainly through the voltage stability and nonlinear dynamics of power systems. In the field of power system planning, he has focused on the influence of inverter-based resources on power systems. In addition, he has worked on wide-area monitoring systems and oscillation monitoring for power system operation.